Catalysis Letters (2019) 149:2930–2939
https://doi.org/10.1007/s10562-019-02805-8

G-C_3N_4 Nanosheets Coupled with TiO_2 Nanosheets as 2D/2D Heterojunction Photocatalysts Toward High Photocatalytic Activity for Hydrogen Production

Yuhao Yang[1,2] · Xiaolong Li[1,2] · Chan Lu[3] · Wenhuan Huang[1,2]

Received: 17 February 2019 / Accepted: 24 April 2019 / Published online: 8 May 2019

Abstract

TiO_2/g-C_3N_4 2D/2D heterojunction nanocomposites were successfully synthesized through a facile self-assembly method. The structure characterization results shows good interaction between TiO_2 nanosheets and g-C_3N_4 nanosheets. The photocatalytic activity of TiO_2/g-C_3N_4 samples were measured by hydrogen production in water splitting under visible light irradiation, which was found that the composites enhance the photocatalytic activity clearly compared to pure g-C_3N_4 and TiO_2 nanosheets. The results could attribute to the formation of 2D heterojunction because of the stimulative charge transfer, promotional separation efficiency of photoexcited electron and hole and the suitable band positions. Besides, the samples exhibited substantial stability under visible light irradiation by the recycling experiments. The feasible photocatalytic mechanism was minutely discussed, which could explain the enhanced photocatalytic activity.

Graphical Abstract

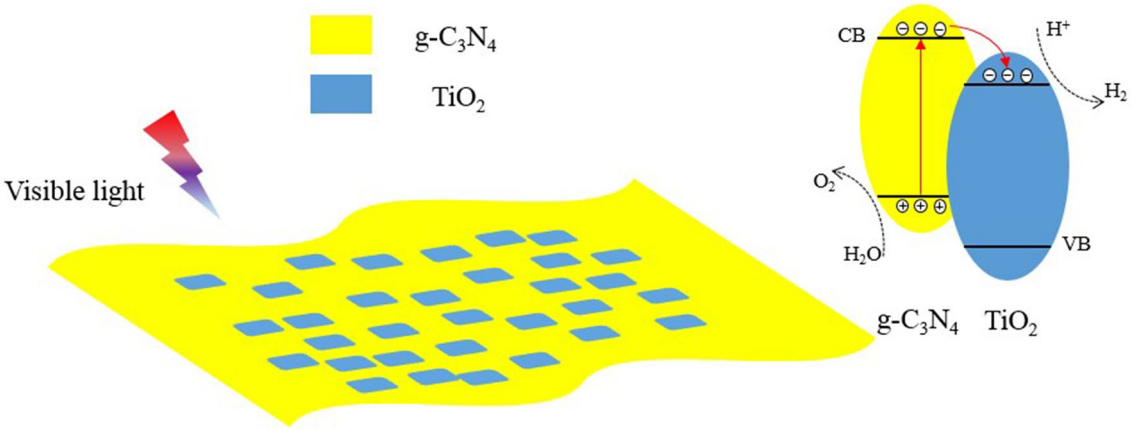

Keywords 2D heterojunction · g-C_3N_4 nanosheets · TiO_2 nanosheets · Photocatalysis · Hydrogen production

1 Introduction

As solar energy is an environmental friendly and an inexhaustible energy resource, semiconductor photocatalysis is a potential strategy for hydrogen production [1–3]. During the past few years, miscellaneous semiconductors such as sulfides [4, 5], metal oxides [6–9] and oxynitride [10, 11] have been studied to drive photocatalytic reaction.

Electronic supplementary material The online version of this article (https://doi.org/10.1007/s10562-019-02805-8) contains supplementary material, which is available to authorized users.

✉ Yuhao Yang
yangyuhao@sust.edu.cn

Extended author information available on the last page of the article

However, their applications have been restricted to a great scope in the environmental purification on account of the low use ratio of visible light and the low efficiency of charge separation. Hence, to improve the efficiency of solar energy utilization, development of suitable semiconductors is a key factor for practical use of this technology. Up to now, it is still a huge challenge to exploit efficient photocatalysts that possess sufficient absorption of visible light and have efficient charge separation.

Graphitic carbon nitride (g-C_3N_4), as a typical n-type semiconductor, has become a new research hotspot in the field of photocatalytic hydrogen production on account of nontoxicity, cheapness, chemical and thermal stability, tunable electronic structure, especially the appropriate band position [12–14]. However, g-C_3N_4 has weak catalytic activity due to the low charge separation efficiency, which seriously restrict the applications [15–17]. To resolve the problem, multiple strategies have been devised such as metals or nonmetals doping [18–20], metal deposition [21, 22], synthesis of porous g-C_3N_4 [23], and preparation of heterojunction composite [24–28]. In these strategies, heterogeneous nanostructures is regarded as the effective and promising strategy, which could enhance the light absorption and photoexcited electron–hole pairs separation. The g-C_3N_4 nanosheets coupled with another semiconductor especially the 2D nanomaterials could promote the charge transfer and separation efficiency of photoexcited electron and hole because of the largest contact area of three types of heterojunction [29–34]. In addtion, layered nanostructure could decrese the spread distance and time of photoinduced carrier. Hence, it is significative to couple the 2D semiconductors heterojunction to prepare more efficient photocatalyst. Regarding the heterogeneous junction, TiO_2 is deemed as one of the applicable choices for binding C_3N_4 due to its proper band structure, low cost and chemical stability [35]. For this purpose, TiO_2 nanoparticles loaded on bulk g-C_3N_4 have been prepared to enhanced the TiO_2 and g-C_3N_4 photocatalytic activity [36–38]. However, synthesis of TiO_2/g-C_3N_4 2D heterojunction photocatalyst has rarely been reported.

Coupling g-C_3N_4 nanosheets with TiO_2 nanosheets is a candidate choice to prepare 2D/2D heterojunction on account of their appropriate band gap, and the position of conduction and valence band. In this paper, 2D TiO_2/g-C_3N_4 heterojunction phototcatalyst were constructed by a self-assembly method. The as-prepared phototcatalyst showed advanced reactivity in hydrogen production under visible light illumination (> 420 nm) compared with pure g-C_3N_4 and TiO_2. Besides, the stability of 2D TiO_2/g-C_3N_4 heterojunction phototcatalyst was researched by the recycling experiments. Finally, the feasible mechanism was minutely discussed.

2 Experimental

2.1 Synthesis of the Photocatalysts

The g-C_3N_4 nanosheets (CNs) were prepared by the ultrasonication of bulk g-C_3N_4, which obtained by the calcination of dicyandiamide [29]. TiO_2 nanosheets (TNs) were synthesized based on literature method (Supplementary Material) [39].

The 2D TiO_2/g-C_3N_4 heterojunction phototcatalyst were prepared by a self-assembly method. 0.05 g CNs was dispersed into 100 mL ethanol with sonicating 60 min to form a glutinous solution. Suitable amount of TNs was dispersed into 100 mL ethanol with sonicating 30 min to form solution. Then, TNs soulation was added into CNs solution drop by drop and stirred for 12 h, after which the hybrid was heated at 70 °C to remove the solvent under stirring. In the end, the product was heated at 400 °C for 4 h to further strengthen the heterojunction interface. The procured 2D TiO_2/g-C_3N_4 heterojunction photocatalyst with different TiO_2 mass contents about 5%, 10%, 15%, 20%, 25% and 30% were donated as TCNNs-5, TCNNs-10, TCNNs-15, TCNNs-20, TCNNs-25 and TCNNs-30, respectively.

2.2 Characterization

The morphologies was observed by FEI Tecnai G2 F20 S-TWIN transmission electron microscopy (TEM) and FEI Verios 460 scanning electron microscope (SEM). The X-ray diffraction (XRD) patterns were determined on a Bruker D8 Advance X-ray diffractometer (Cu Kα radiation). X-ray photoelectron spectroscopy (XPS) characterization was obtained with Kratos AXIS SUPRA spectrometer. The photoluminescence (PL) spectra were measured by Hitachi F-7000 fluorescence spectrometer and the transient PL spectra were measured by Edinburgh FS35 fluorescence spectrometer. The UV–Vis absorption spectra were recorded on a Shimadzu UV-3600 spectrophotometer. The Brunauer–Emmett–Teller (BET) surface area (S_{BET}) of the powders was analyzed by nitrogen adsorption in an ASAP2020 surface area and porosity analyzer (Micromeritics, USA). All the samples were degassed at 150 °C prior to nitrogen adsorption measurements. The BET surface area was determined by a multipoint BET method using the adsorption data in the relative pressure (P/P_0) range of 0.05–0.25.

The photocurrents were measured with a CHI660E electrochemical workstation in a standard three electrode cell, where a Pt wire was employed as counter electrode, Hg/Hg_2Cl_2 was used as a reference electrode. A 150 W

Xe lamp was used as the light source and 0.5 M Na_2SO_4 aqueous solution was used as the electrolyte. The modified electrode was prepared as follows: 15 mg sample was mixed with 1 mL ethanol and 0.15 mL solution was dropped onto the ITO and then dried at 60 °C for 6 h.

2.3 Evaluation of Photocatalytic Performance

The photocatalytic H_2 production was performed in a 150 mL quartz reactor. A Xenon lamp with a cutoff filter ($\lambda > 420$ nm) as the light source was placed at outside 35 cm away from of the quartz reactor. The sample was firstly dispersed in mixed aqueous solution containing 8 mL ethanol and 72 mL H_2O. Then the mixed aqueous solution was positioned faced to the lamp. The system was evacuated by bubbling nitrogen for 30 min before light irradiation, then illuminated for 6 h with magnetic stirring. 1 mL of reactive gas was taken from the reactor with a syringe for analysis via gas chromatography (Beifen 3420 A, TCD, N_2 carrier).

3 Results and discussion

3.1 XRD analysis

The X-ray diffraction patterns of pure CNs, TNs and all composite are shown in Fig. 1. CNs exhibits two basic peaks at 12.9° and 27.5°. which can be indicated as the (100) and (002) diffraction planes (JCPDS 87-1526). The peak with weaker intensity at 12.9° relates to in-plane structural packing motif, while the strong peak at 27.5° corresponds to long-range inter planar stacking of aromatic systems. TNs exhibits three main diffraction peaks at 25.2°, 37.7°, and 48°, which can be indicated as the (101), (004) and (200) diffraction planes of anatase-phase TiO_2 (JCPDS 21-1272). The results have shown that the main phase of as-prepared sample is anatase TiO_2. Additionally, the diffraction peaks of all TCNs samples are in good agreement with CNs and TNs, which shows interaction between CNs and TNs. Besides, the peak intensities of TCNs samples are weaker than that of CNs, which may due to the small amount of TiO_2 contents.

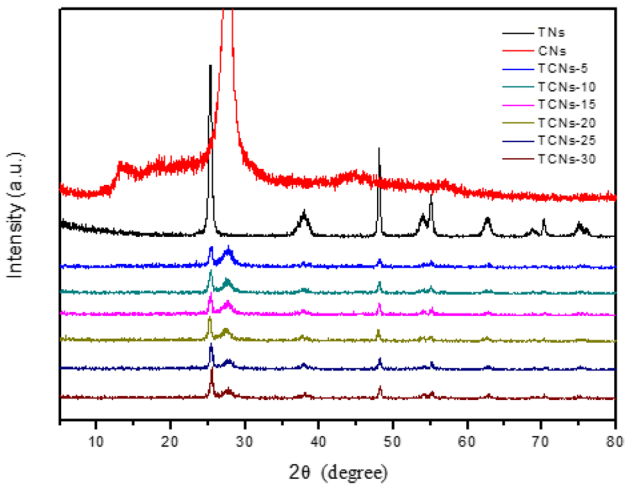

Fig. 1 XRD patterns of TCNs composite, pure TNs and pure CNs

3.2 TEM and HRTEM Analysis

TEM images of the pure TNs, CNs and TCNs-20 samples are shown in Fig. 2. Figure 2a have shown the TNs well-defined plate-like structure, of which grain diameter is about 50 nm. Figure 2b shows CNs nanosheets structure, which give facts that the CNs are monolayers or few layers. Figure 2c shows the TEM image of the TCNs-20, which reveals the 2D heterostructure by TNs and CNs. The TNs were horizontal loaded on the CNs with close interfacial contact. It is deserve to be mentioned that the 2D structure leads to the increase in the contact area effectively. Figure 2d is the detailed structure of the TCNs-20. As shown in Fig. 2d, the lattice distance of 0.351 nm, corresponding to the (101) plane of anatase TiO_2, indicating the formation of 2D TiO_2/g-C_3N_4 heterojunction. To further corroborate the element distribution of TiO_2/g-C_3N_4 composites, the elemental mapping of TCNs-20 was performed. The results (Fig. 2e) reveal that the Ti, O, C and N elements exist in the composite. It can be seen that the elements of Ti and O are well overlapped with the C and N element in the contact part of TNs and CNs, further confrming the 2D/2D interfacial interaction between TNs and CNs.

3.3 XPS Analyze

XPS measurements were performed to explicate the chemical components and the states in the heterostructure. As the Fig. 3a shows, the C 1s peak at 284.6 eV is corresponded to graphitic carbon. The other C1s peak at 288.4 eV is assigned to sp^2-bonded carbon in the striazine rings. In addition, the peak at 286.1 eV is associated with organic C–O in the g-C_3N_4. Figure 3b shows the N 1s spectrum. There are three fitted peaks at 398.4 eV, 400.0 eV and 401.5 eV, which could put down to C–N–C, N–$(C)_3$, and N–H [29]. Two typical peaks of Ti 2p located at approximately 458.9 and 464.5 eV are assigned to the Ti $2p_{3/2}$ and Ti $2p_{1/2}$, respectively. In Fig. 3d, the two main peaks of 529.8 and 532.1 eV are ascribed to the O 1s. The binding energy at 533–534 eV figures organic C=O from g-C_3N_4. The above mentioned observations indicate that the 2D heterostructure between TiO_2 nanosheets and g-C_3N_4 nanosheets were successfully prepared.

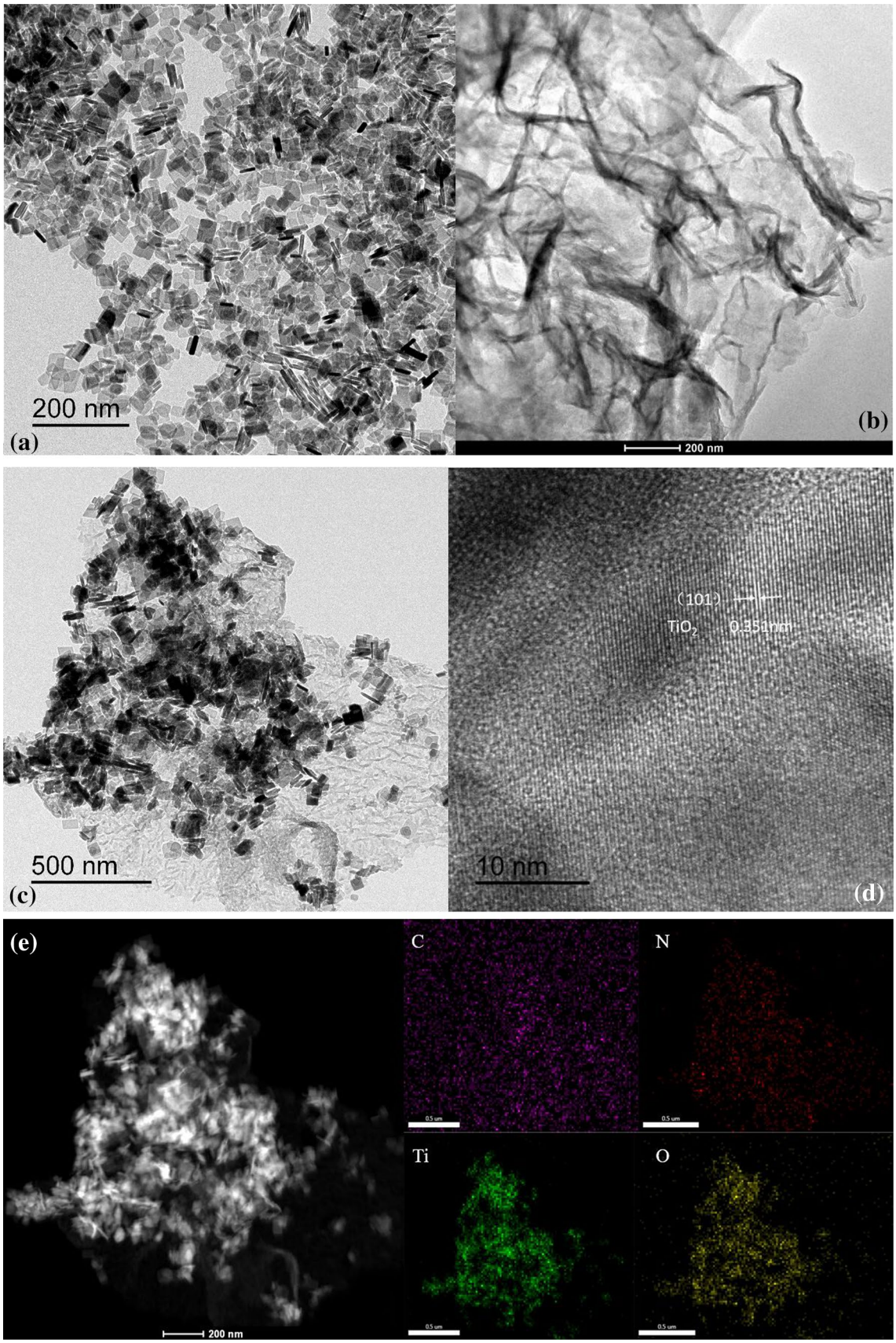

Fig. 2 TEM images of **a** TNs, **b** CNs, **c** TCNs-20; HRTEM image of **d** TCNs-20; EDX-Mapping image of **e** TCNs-20

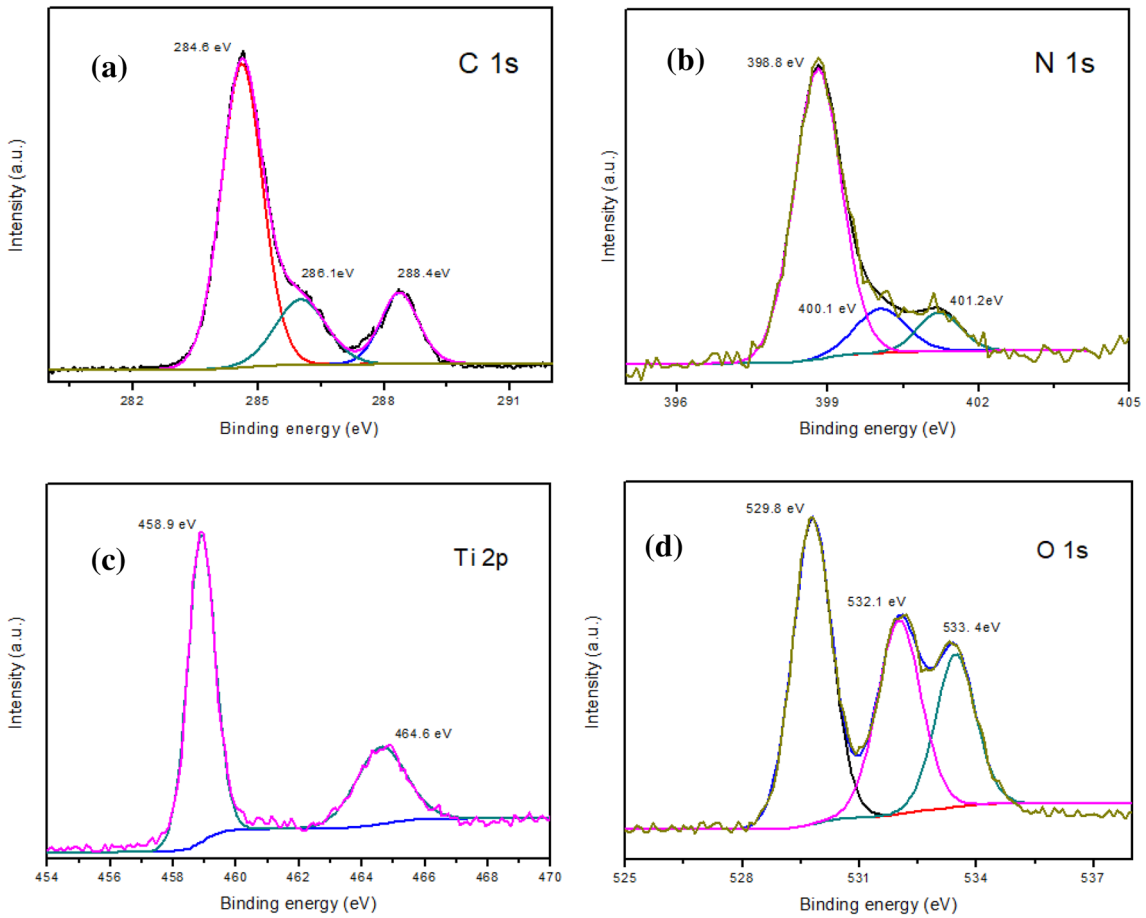

Fig. 3 High-resolution XPS C 1s, N 1s, Ti 2p and O 1s spectra of TCNs-20

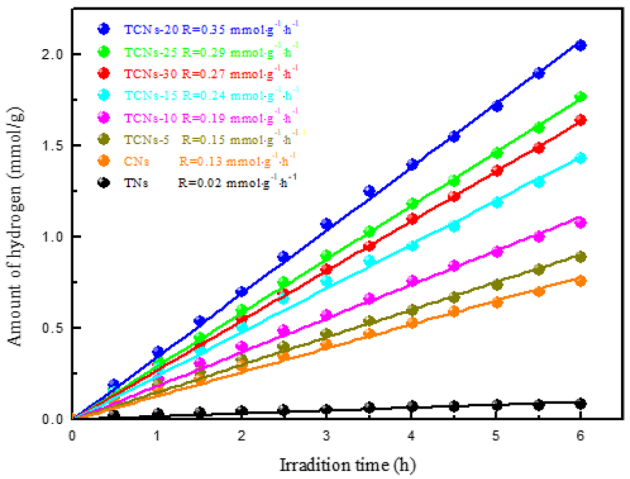

Fig. 4 Photocatalytic H_2 evolution of different samples

3.4 Photocatalytic Activity and Mechanism

Photocatalytic H_2 production in visible light is accomplished to inquire into the photocatalytic activity of the samples, which are shown in Fig. 4. Pure TNs shows only 0.02 mmol g^{-1} h^{-1} H_2 production rate and the H_2 production rate of pure CNs is about 0.13 mmol g^{-1} h^{-1}. By comparison, the composite samples have a higher H_2 production rate. When CNs is ornamented with 5 wt% of TCNs, the H_2 production rate is significantly increased to 0.15 mmol g^{-1} h^{-1}. In addition, the H_2 production rate of composite sample attains the highest at 0.35 mmol g^{-1} h^{-1} when the TNs increased to 20 wt%, which is 2.7 times higher than that of pure CNs. The increasement in photocatalytic H_2 production activity mainly on account of the formed close interfaces between the sheet-like TNs and CNs. This sheet-like structure interfaces can not only promote charge separation effectively, but also inhibit recombination of photogenerated electron–hole pairs in CNs nanosheets. Besides, the results of H_2 production rate is even better than the MoS_2 quantum dots/g-C_3N_4 heterostructure photocatalyst [40], which indicates TNs is an ideal candidate choice to prepare heterojunction with g-C_3N_4. Nevertheless, extra TNs may restrict the light absorption of CNs and also could be the combination center of photo-generated carriers, bringing out

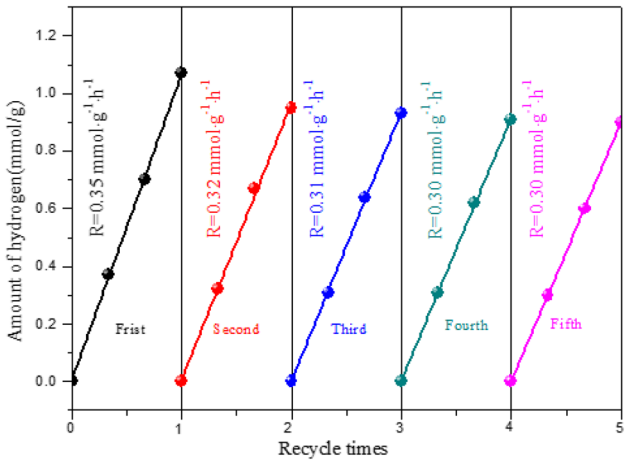

Fig. 5 Cycling runs for five times in the photocatalytic hydrogen production by TCNs-20

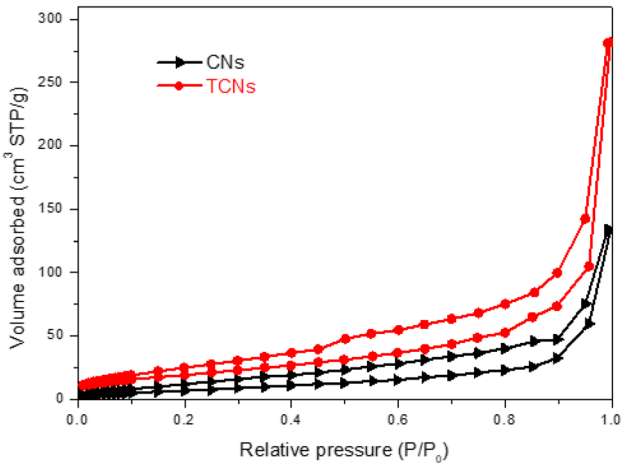

Fig. 7 Nitrogen adsorption–desorption isotherms of CNs and TCNs

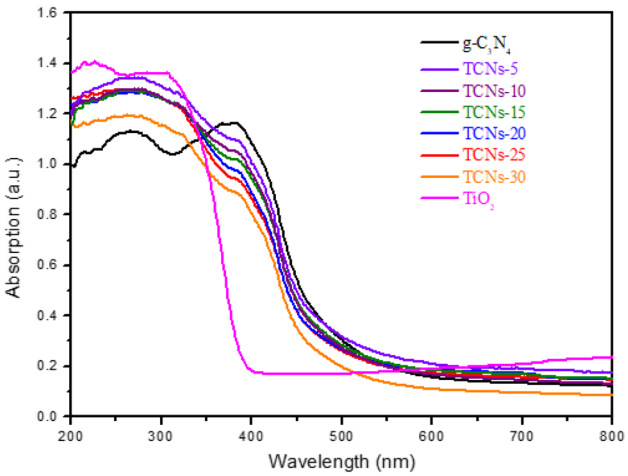

Fig. 6 UV–Vis diffuse reflectance spectra of different samples

a depressed photocatalytic activity. Figure 5 shows that the prepared photocatalyst is greatly stable in recycling experiments.

Generally speaking, light absorption and charge transfer have strong impact on photocatalytic performance [41–43]. Figure 6 shows the UV–vis diffuse reflectance spectra of the samples. The pure TNs shows a sharp absorption increase at ~ 390 nm and the pure CNs shows a sharp absorption increase at ~ 490 nm in the visible light region, which is well accord with the band gap of TO_2 and g-C_3N_4. The composite materials have distinct absorption in visible light region. Interestingly, the absorption intensity at visible region is apparently subdued with increasing TNs contents, which may suggest that proper contents of TNs in the composite is required.

Figure 7 displays the the nitrogen adsorption/desorption isotherms of the asobtained samples. The tested CNs and TCNs materials exhibited type IV isotherms with H_3 hysteresis loops, which was characteristic of mesoporous materials. The calculated specific surface areas of the TCNs-20 were 29.55 $m^2\ g^{-1}$, which is about 2.4 times larger than that of CNs (72.15 $m^2\ g^{-1)}$, suggesting the TCNs-20 could provide more active sites for photocatalytic H_2 producntion. As a result, TCNs-20 exhibited the greatly enhanced photocatalytic activity. Figure 8a shows the photoluminescence spectra of CNs and TCNs-20 composite samples, which are registered with an excitation wavelength of 370 nm. PL is quenched in TCNs composites, demonstating the recombination of photoexcited electrons-holes pairs is restrained obviously in the composite samples. The PL quenching can be attributed to the enhanced charge transfer between the TNs and CNs faces. The charge transfer could be further affirmed by transient photoluminescence spectra, as displays in Fig. 8b. The TCNs shows a shorter decay time τ value 7.98 ns than CNs (10.52 ns), related to a nonradiative pathway and rapid interfacial electron injection efficiency at the 2D in-plane (inset of Fig. 8b, eqn S6). Figure 9a shows the transient photocurrent responses of CNs and TCNs-20 composite samples. The photocurrent of TCNs-20 is apparently higher than that of the CNs. The enhanced photocurrent indicates the 2D heterojunction could boost the efficiency of charge transfer and separation. The electrochemical impedance spectroscopy was carried out to further investigate charge transfer and recombination processes, and the result was shown in Fig. 9b. Compared with CNs, the smaller arc radius on the EIS Nyquist plot of TCNs-20 observed, which indicated a more effective separation of photogenerated electron–hole pairs and a faster interfacial charge transfer had occurred on the surface. The EIS results were consistent with the photocurrents analysis, which further confirm that the presence of TNs was beneficial to separation of electron–hole pairs, thus leading to improved photocatalytic

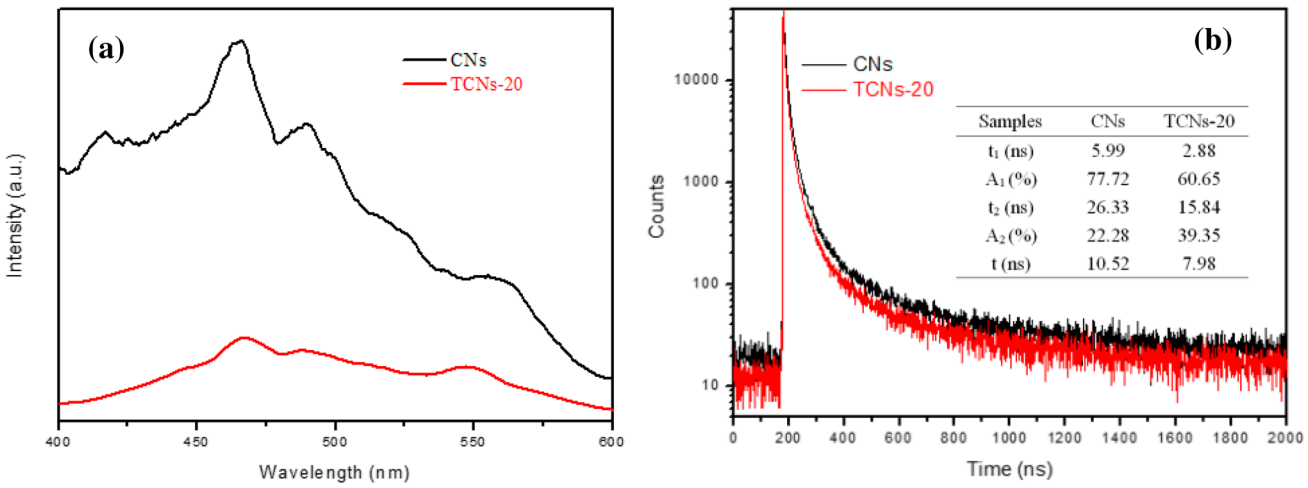

Fig. 8 **a** PL spectra and **b** transient PL spectra of CNs and TCNs-20

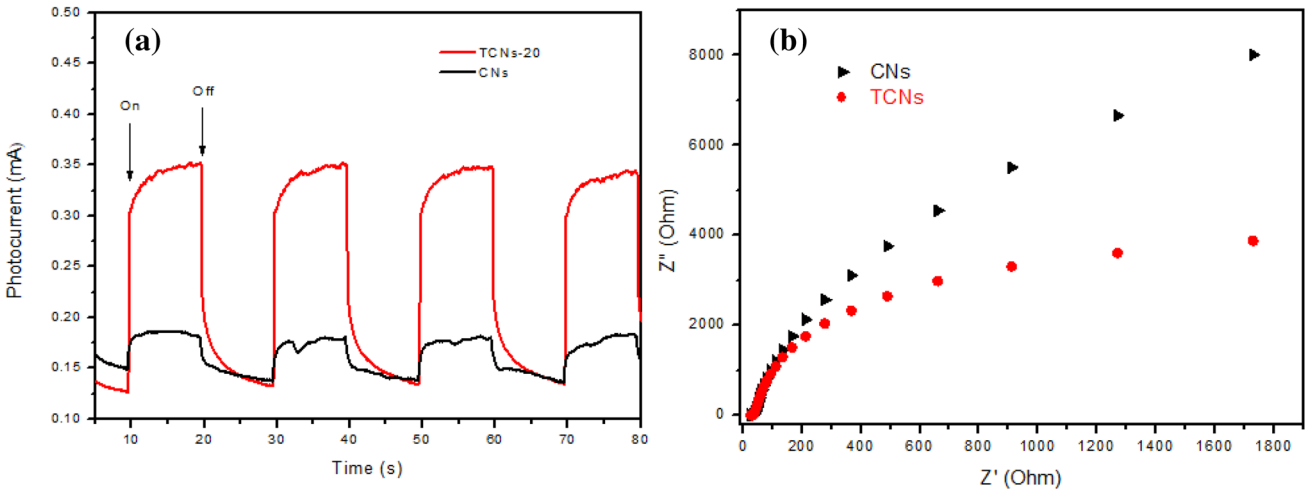

Fig. 9 **a** Transient photocurrent responses, **b** electrochemical impedance spectroscopy of CNs and TCNs-20

activities. From the above, the introduction of TNs on the surface of CNs could improve the photoinduced electron–hole pairs separated efficiently, which could enhance the photocatalytic performances.

The photocatalytic process is discussed to reveal the proposed mechanism using the 2D TiO_2/g-C_3N_4 composites and schematically illustrated in Scheme 1. As is well known that the band gap could be estimated by extrapolating to zero with a linear fit to the plot of the square root of Kubelka–Munk function against hν of the light (Fig. 10a). The band gap of TNs was estimated to be ca. 3.33 eV, which was a little bigger than that of P25 (3.2 eV). The band gap of CNs was estimated to be ca. 2.84 eV. In addition, as shown in the Fig. 10b of XPS valence band energy spectra, the valence band (VB) of TNs and CNs was 2.78 eV and 1.74 eV, respectively. When TNs were introduced onto the CNs, the two material combined together closely. Thus, the energy bands between TNs and CNs is matched. Under visible light irradiation, CNs could be easily excited to produce photo-generated electron–hole pairs. On account of the CB potential of CNs is more negative than that of TNs, the photoexcited electrons in the CB of CNs could transfer to that of the TNs through the interface easily, which bring about photoexcited electrons and holes separated effectively. As a consequence, the electrons are assembled in the CB of TNs and the holes in the VB of CNs. Hence, the electron–hole recombination is hindered. Thus, the H_2-evolution apparent quantum efficiency of the TCNs-20 was measured, which was about 4.99% at 420 nm (Supplementary Material, eqn (S5)).

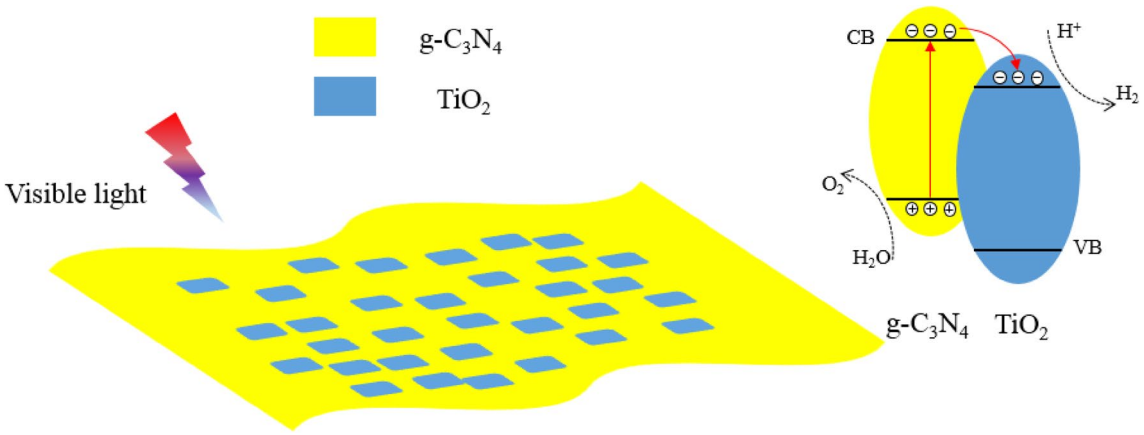

Scheme 1 Schematic diagram of photocatalytic mechanism of the 2D TiO_2/g-C_3N_4 composites

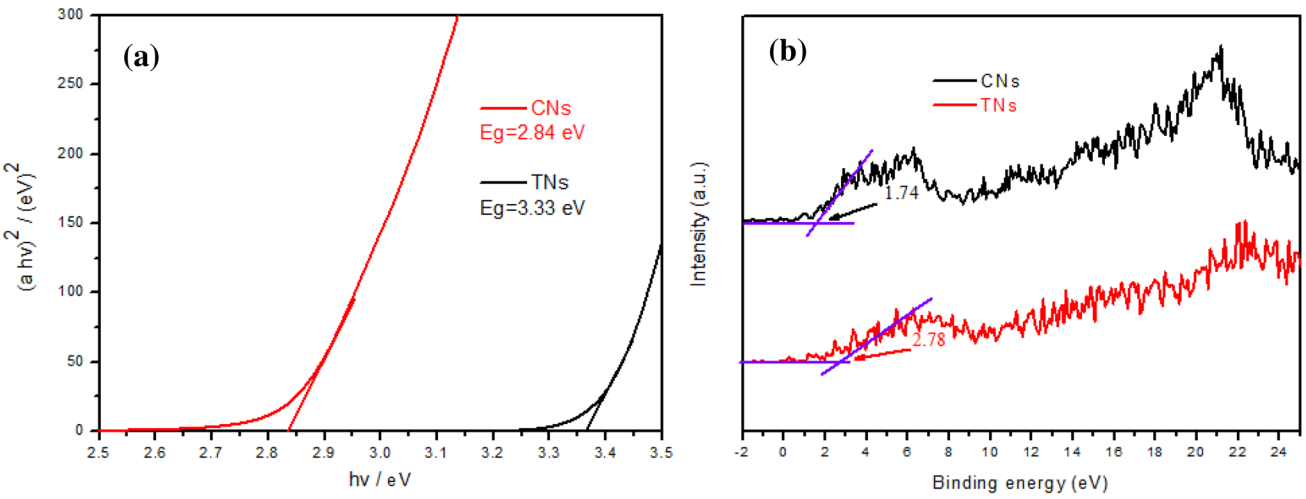

Fig. 10 **a** Spectrum expressed as the Kubelka–Munk function and **b** The valence band energy spectra of TNs and CNs

4 Conclusions

In summary, TiO_2/g-C_3N_4 2D/2D heterojunction nanocomposites were successfully synthesized through a facile self-assembly method The 2D heterojunction enhances the photocatalytic performance apparently in hydrogen production under visible light irradiation. The results could be attributed to the formation of 2D heterojunction because of the stimulative charge transfer, promotional separation efficiency of photoexcited electron and hole and the suitable band positions. This study highlights that the 2D heterojunction photocatalyst will be a prospective method to product hydrogen by using solar energy efficiently.

Acknowledgments This work supported by the Scientific Research Foundation of Shaanxi University of Science & Technology (No. BJ14-24), Special Research Fund of Education Department of Shaanxi (No. 15JK1105, 16JK1108) and Research Fund of Technology Department of Shaanxi (No. 2017JQ2021).

References

1. Li X, Yu J, Low J, Fang Y, Xiao J, Chen X (2015) Engineering heterogeneous semiconductors for solar water splitting. J Mater Chem A 3:2485–2534
2. Kudo A, Miseki Y (2009) Heterogeneous photocatalyst materials for water splitting. Chem Soc Rev 38:253–278
3. Li X, Yu J, Jaroniec M, Chen X (2019) Cocatalysts for selective photoreduction of CO_2 into solar fuels. Chem Rev. https://doi.org/10.1021/acs.chemrev.8b00400
4. Li X, Dong H, Wang B, Lv J, Xu G, Wang D, Wu Y (2018) Controllable synthesis of MoS_2/h-CdS/c-CdS nanocomposites with enhanced photocatalytic hydrogen evolutionu under visible light irradiation. Catal Lett 148:3445–3453

5. Yang H, Liu Z, Wang K, Pu S, Yang S, Yang L (2017) A facile synthesis of TiO_2-CdS heterostructures with wnhanced photocatalytic activity. Catal Lett 147:2581–2591
6. Hu Y, Pan W, Kong X (2018) Enhancement of photocatalytic activity for fold-like ZnO via hybridization with grapheme. Micro Nano Lett 13:232–236
7. Yang Y, Huang W (2018) Design of copper and titanium dioxide nanoparticles doped with reduced graphene oxide for hydrogen evolution by water splitting. Russ J Phys Chem A 92:968–975
8. Fakhri A, Behrouz S (2015) Photocatalytic properties of tungsten trioxide (WO_3) nanoparticles for degradation of Lidocaine under visible and sunlight irradiation. Sol Energy 112:163–168
9. Khan H, Murtaza G, Choudhary M, Ahmed Z, Malik M (2018) Photocatalytic removal of carcinogenic reactive red S3B dye by using ZnO and Cu doped ZnO nanoparticles synthesized by polyol method: a kinetic study. Sol Energy 173:875–881
10. Nakamura R, Tanaka T, Nakato Y (2005) Oxygen photoevolution on a tantalum oxynitride photocatalyst under visible-light irradiation: how does water photooxidation proceed on a metal-oxynitride surface? J Phys Chem B 109:8920–8927
11. Yashima M, Maeda K, Teramura K, Takata T, Domen K (2005) Crystal structure and optical properties of (Ga1-xZnx)(N1-xOx) oxynitride photocatalyst (x = 0.13). Chem Phys Lett 416:225–228
12. Naseri A, Samadi M, Pourjavadi A, Moshfegh A (2017) Graphitic carbon nitride (g-C_3N_4)-based photocatalysts for solar hydrogen generation: recent advances and future development directions. J Mater Chem A 5:23406–23433
13. Lu X, Xie J, Liu S, Adamski AJ, Chen X, Li X (2018) Low-cost $Ni_3B/Ni(OH)_2$ as an ecofriendly hybrid cocatalyst for remarkably boosting photocatalytic H_2 production over g-C_3N_4 nanosheets. Acs Sustain Chem Eng 6:13140–13150
14. Wen J, Xie J, Yang Z, Shen R, Li H, Luo X, Chen X, Li X (2017) Fabricating the robust g-C_3N_4 nanosheets/carbons/NiS multiple heterojunctions for enhanced photocatalytic H_2 generation: an insight into the trifunctional roles of nanocarbons. Acs Sustain Chem Eng 5:2224–2236
15. Ong W, Tan L, Yun H, Yong S, Chai S (2016) Graphitic carbon nitride (g-C_3N_4)-based photocatalysts for artificial photosynthesis and environmental remediation: are we a step closer to achieving sustainability? Chem Rev 116:7159–7329
16. Lakhi K, Park D, Al-Bahily K, Cha W, Viswanathan B (2016) Mesoporous carbon nitrides: synthesis, functionalization, and applications. Chem Soc Rev 46:72–101
17. Wen J, Xie J, Chen X, Li X (2017) A review on g-C_3N_4-based photocatalysts. Appl Surf Sci 391:72–123
18. Liu G, Niu P, Sun C, Smith SC, Chen Z (2010) Unique electronic structure induced high photoreactivity of sulfur-doped graphitic C_3N_4. J Am Chem Soc 132:11642–11648
19. Oh Y, Hwang J, Lee E, Yoon M, Le V, Kim Y, Kim D, Kim S (2016) Divalent Fe atom coordination in two-dimensional microporous graphitic carbon nitride. ACS Appl Mater Interfaces 8:25438–25443
20. Jiang J, Cal S, Hu C, Chen C (2017) A comparison study of alkali metal-doped g-C_3N_4 for visible-light photocatalytic hydrogen evolution. Chin J Catal 38:1981–1989
21. Caux M, Fina F, Irvine J, Idriss H, Howe R (2017) Impact of the annealing temperature on Pt/g-C_3N_4, structure, activity and selectivity between photodegradation and water splitting. Catal Today 281:182–188
22. Patnaik S, Martha S, Madras G, Parida K (2016) Effect of sulfate pre-treatment to improve deposition of Au-nanoparticles in sulphated g-C_3N_4 photocatalyst towards visible light induced water reduction reaction. Phys Chem Chem Phys 18:28502–28514
23. Zhu B, Xia P, Ho W, Yu J (2015) Isoelectric point and adsorption activity of porous g-C_3N_4. Appl Surf Sci 344:188–195
24. Yu J, Nong Q, Jiang X, Liu X, Wu Y, He Y (2016) Novel $Fe_2(MoO_4)_3$/g-C_3N_4 heterojunction for efficient contaminant removal and hydrogen production under visible light irradiation. Sol Energy 139:355–364
25. Chen F, Yang H, Wang X, Yu H (2017) Facile synthesis and enhanced photocatalytic H_2-evolution performance of NiS_2-modified g-C_3N_4 photocatalysts. Chin J Catal 38:296–304
26. He K, Xie J, Luo X, Wen J, Ma S, Li X, Fang Y, Zhang X (2017) Enhanced visible light photocatalytic H_2 production over Z-scheme g-C_3N_4 nansheets/WO_3 nanorods nanocomposites loaded with $Ni(OH)_x$ cocatalysts. Chin J Catal 38:240–252
27. Shen R, Liu W, Ren D, Xie J, Li X (2019) $Co_{1.4}N_{i0.6}P$ cocatalysts modified metallic carbon black/g-C_3N_4 nanosheet Schottky heterojunctions for active and durable photocatalytic H_2 production. Appl Surf Sci 466:393–400
28. Wang J, Xia Y, Zhao H, Wang G, Xiang L, Xu J, Komarneni S (2017) Oxygen defects-mediated Z-scheme charge separation in g-C_3N_4/ZnO photocatalysts for enhanced visible-light degradation of 4-chlorophenol and hydrogen evolution. Appl Catal B 206:406–416
29. Li J, Liu E, Ma Y, Hu X, Wan J, Sun L, Fan J (2016) Synthesis of MoS_2/g-C_3N_4 nanosheets as 2D heterojunction photocatalysts with enhanced visible light activity. Appl Surf Sci 364:694–702
30. Jo W, Kumar S, Eslava S, Tonda S (2018) Construction of Bi_2WO_6/RGO/g-C_3N_4 2D/2D/2D hybrid Z-scheme heterojunctions with large interfacial contact area for efficient charge separation and high-performance photoreduction of CO_2 and H_2O into solar fuels. Appl Catal B 239:586–598
31. Fu F, Xu Q, Low J, Jiang C, Yu J (2019) Ultrathin 2D/2D WO_3/g-C_3N_4 step-scheme H_2-production photocatalyst. Appl Catal B 243:556–565
32. Xu Q, Zhu B, Jiang C, Cheng B, Yu J (2019) Constructing 2D/2D Fe_2O_3/g-C_3N_4 direct Z-Scheme photocatalysts with enhanced H_2 generation performance. Solar RRL 2:1800006
33. Ran J, Guo W, Wang H, Zhu B, Yu J, Qiao S-Z (2018) Metal-free 2D/2D phosphorene/g-C_3N_4 Van der Waals heterojunction for highly enhanced visible-light photocatalytic H_2 production. Adv Mater 30:1800128
34. Wang Q, Wang W, Zhong L, Liu D, Cao X, Cui F (2018) Oxygen vacancy-rich 2D/2D BiOCl-g-C_3N_4 ultrathin heterostructure nanosheets for enhanced visible-light-driven photocatalytic activity in environmental remediation. Appl Catal B 220:290–302
35. Li Y, Wang R, Li H, Wei X, Feng J, Liu K, Dang Y, Zhou A (2015) Efficient and stable photoelectrochemical seawater splitting with TiO_2@g-C_3N_4 nanorod arrays decorated by Co-Pi. J Phys Chem C 119:20283–20292
36. Zhou J, Zhang M, Zhu Y (2015) Photocatalytic enhancement of hybrid C_3N_4/TiO_2 prepared via ball milling method. Phys Chem Chem Phys 17:3647–3652
37. Yu J, Wang S, Low J, Xiao W (2013) Enhanced photocatalytic performance of direct Z-scheme g-C_3N_4–TiO_2 photocatalysts for the decomposition of formaldehyde in air. Phys Chem Chem Phys 15:16883–16890
38. Lei J, Chen Y, Wang L, Liu Y, Zhang J (2015) Highly condensed g-C_3N_4-modified TiO_2 catalysts with enhanced photodegradation performance toward acid orange 7. J Mater Sci 50:3467–3476
39. Xu H, Li S, Ge L, Han C, Gao Y, Dai D (2017) In-situ synthesis of novel plate-like $Co(OH)_2$ co-catalyst decorated TiO_2 nanosheets with efficient photocatalytic H_2 evolution activity. Int J Hydrog Energy 42:22877–22886
40. Liu Y, Zhang H, Ke J, Zhang J, Tian W, Xu X, Duan X, Sun H, Tade M, Wang S (2018) 0D (MoS_2)/2D (g-C_3N_4) heterojunctions in Z-scheme for enhanced photocatalytic and electrochemical hydrogen evolution. Appl Catal B 228:64–74
41. Cao S, Yu J (2014) G-C_3N_4-based photocatalysts for hydrogen generation. J Phys Chem Lett 5:2101–2107

42. Xu J, Zhang L, Shi R, Zhu Y (2013) Chemical exfoliation of graphitic carbon nitride for efficient heterogeneous photocatalysis. J Mater Chem A 1:14766–14772
43. Li W, Zhao C, Zhang Q (2018) Synthesis of Bi/BiOCl-TiO_2-CQDs quaternary photocatalyst with enhanced visible-light photoactivity and fast charge migration. Catal Commun 107:74–77

Affiliations

Yuhao Yang[1,2] · Xiaolong Li[1,2] · Chan Lu[3] · Wenhuan Huang[1,2]

[1] The School of Chemistry & Chemical Engineering, Shaanxi University of Science & Technology, Xi'an 710021, China

[2] Shaanxi Key Laboratory of Chemical Additives for Industry, Shaanxi University of Science and Technology, Xi'an 710021, China

[3] Architectural Engineering Institute, Shaanxi Energy Insititute, Xianyang 712000, China